Acta Polytechnica **57**(3):167–181, 2017
doi:10.14311/AP.2017.57.0167

available online at http://ojs.cvut.cz/ojs/index.php/ap

DESIGN AND CONSTRUCTION OF A PROTOTYPE SOLAR UPDRAFT CHIMNEY IN ASWAN/EGYPT

Reinhard Harte[a,*], Markus Tschersich[b], Rüdiger Höffer[c], Tarek Mekhail[d]

[a] *Faculty of Architecture and Civil Engineering, University of Wuppertal, Pauluskirchstraße 7, 42285 Wuppertal, Germany*

[b] *Faculty of Architecture and Civil Engineering, University of Wuppertal, Pauluskirchstraße 7, 42285 Wuppertal, Germany*

[c] *Ruhr-Universität Bochum, Department of Civil and Environmental Engineering, Universitätsstraße 150, 44801 Bochum, Germany*

[d] *Faculty of Energy Engineering, Aswan University, Sahary City, 81528 Aswan, Egypt*

[*] corresponding author: harte@uni-wuppertal.de

Abstract. This work is part of a joint project funded by the Science and Technology Development Fund (STDF) of the Arab republic of Egypt and the Federal Ministry of Education and Research (BMBF) of the Federal Republic of Germany. Continuation of the use of fossil fuels in electricity production systems causes many problems such as: global warming, other environmental concerns, the depletion of fossil fuels reserves and continuing rise in the price of fuels. One of the most promising paths to solve the energy crisis is utilizing the renewable energy resources. In Egypt, high insolation and more than 90 percent available desert lands are two main factors that encourage the full development of solar power plants for thermal and electrical energy production. With an average temperature of about 40 °C for more than half of the year and average annual sunshine of about 3200 hours, which is close to the theoretical maximum annual sunshine hours, Aswan is one of the hottest and sunniest cities in the world. This climatic condition makes the city an ideal place for implementing solar energy harvesting projects from solar updraft tower. Therefore, a Solar Chimney Power Plant (SCPP) is being installed at Aswan City. The chimney height is 20.0 m, its diameter is 1.0 m and the collector is a four-sided pyramid, which has a side length of 28.5 m. A mathematical model is used to predict its performance. The model shows that the plant can produce a maximum theoretical power of 2 kW. Moreover, a CFD code is used to analyse the temperature and velocity distribution inside the collector, turbine and chimney at different operating conditions. Static calculations, including dead weight and wind forces on the solar updraft chimney and its solar collector, have been performed for the prototype. Mechanical loading and ambient impact on highly used industrial structures such as chimneys and masts cause lifetime-related deteriorations. Structural degradations occur not only from rare extreme loading events, but often as a result of the ensemble of load effects during the life-time of the structure. A Structural Health Monitoring (SHM), framework for continuous monitoring, is implemented on the solar tower. For the ongoing case study, the types of impacts, the development of the strategic sensor positioning concept, examples of the initially obtained results and further prospects are discussed. Additional wind tunnel tests have been performed to investigate the flow situation underneath the solar collector and inside the transition section. The flow situation in and around the SCPP has been simulated by a combination of the wind tunnel flow and a second flow inside the solar tower. Different wind tunnel velocities and volume flow rates have been measured respectively. Particle Image Velocimetry (PIV) measurements give some indication of the flow situation on the in- and outside of the solar tower and underneath the collector roof. Numerical simulations have been performed with the ANSYS Fluent to validate the experimental tests.

Keywords: ANSYS fluent; Aswan; CFD; FDS; mathematical model; permanent vibration measurement; PIV; solar chimney; solar radiation; structural health monitoring and identification; wind tunnel.

1. Introduction

In Egypt, fossil fuel resources mainly dominate the electricity production and burning fuel has a harmful effect on environment that reflects human life. In 1991, the solar atlas for Egypt was issued, indicating that the country enjoys about 2900–3200 hours of sunshine annually, with an annual direct normal energy density 1970–3200 kWh/m^2 and technical solar-thermal electricity generating a potential of 73.6 Petawatt hour (PWh) [1]. Herein, the solar thermal power plants have many advantages, the priorities of consistent power output and the ability to incorporate a storage. The operation of a Solar ChimneyPower Plant (SCPP) is based on a simple principle: when air is heated by the greenhouse effect under the transparent roof, buoyancy force is a consequence of a density variation, less dense hot air rises up a chimney, which is installed at the centre of the collector (as shown in Figure 1). At the base of the chimney, the air flows through the turbine to produce mechanical energy for driving a generator. In 1982, the first pilot plant was built in Spain [2, 3], since then, many prototypes of the SCPP have been built by experts in various countries. Australian engineers intend to construct the largest SCPP in the world with the generation capacity reaching up to 200 MW in New South Wales of Australia. The chimney will be 1000 m in height and the collector will be 7 km in diameter, the system would cover a ground area of 38 km^2 [4]. Currently, this project is postponed indefinitely. Experimental and numerical calculation methods can be used to study the performance of the SCPPs, but the large scale system is hard to establish. However, with the development of a computer technology and Computational Fluid Dynamics (CFD) software techniques, both temperature and pressure distribution in the large system can easily be predicted by a numerical calculation method [5].

Many researchers aimed to optimize the geometry of the major components of the SCPP. In [6], the influence of a changing geometry to improve the flow characteristics inside the SCPP has been studied using the CFD software ANSYS-CFX. The overall chimney height and the collector diameter of the SCPP were kept constant. The collector inlet opening, outlet diameter and the diameter of the chimney were the variables. These modified collectors were tested with chimneys of different divergence angles and different chimney inlet openings. Based on the CFX computational results; the best configuration was achieved using the chimney with a divergence angle of 2°. The authors in [7] used FLUENT software to optimize the SCPP by changing the collector inlet opening and outlet diameter of the chimney, and concluded that the available power was virtually unresponsive to the variation of the collector inlet opening.

More analytical models to predict the performance of solar chimney power plants have been proposed since the early 1980s. In [2], a simple mathematical model that is used for the design of the pilot plant in Manzanares is presented. The authors in [8] have developed comprehensive models to solve the governing conservation and draught equations simultaneously, and [9] presented similar techniques to predict the SCPP performance. The results show that the height of the chimney, the factor of pressure drop at the turbine, the diameter and the optical properties of the collector are important parameters for the design of solar chimneys. The authors of paper [10] adapted the standard gas turbine cycle to define a standard solar chimney cycle. In the analysis, the adaption includes the friction of the chimney, turbine system and exit kinetic energy losses. A more detailed model is offered in [11], which is capable of estimating the temperature and power output of solar chimneys as well as examining the effects of various ambient conditions and structural dimensions on the power output. This mathematical model was verified against their own experimental results and the results of the Manzanares pilot plant [12]. In paper [13], the performance characteristics of large-scale commercial solar chimneys are predicted, indicating that the plant size, the factor of pressure drop at the turbine and solar heat flux were important parameters for performance enhancement that was studied. The collector radius and the chimney height of 200 m and 400 m, respectively, were built in this model study. Furthermore, the optimum ratio between the turbine extraction pressure is shown and the available driving pressure for the proposed plant is approximately 0.84. A simple method to evaluate the turbine power output for solar chimney systems was also proposed in the study using dimensional analysis.

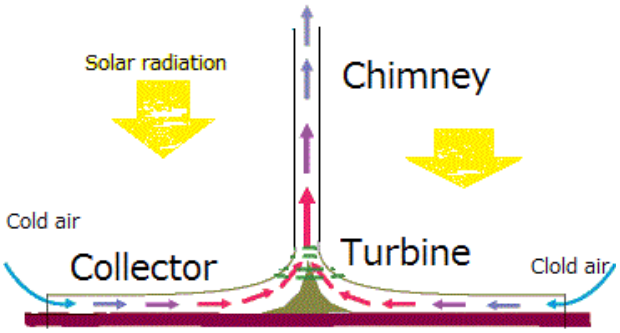

Figure 1. Schematic diagram of the SCPP.

The objective of this study is to accurately analyse the SCPP system by using the mathematical model and the CFD model, fewer assumptions are used in theoretical calculation, but more detailed descriptions of the temperature and flow field could be obtained. A 3D approach for a SCPP prototype is carried out by using the ANSYS CFX v15, which was constructed with the main dimensions as mentioned before. Figure 2 shows the plant that is still under construction. The 3D numerical simulation, incorporating the radiation models and turbine models, is used. Results

FIGURE 2. Prototype in Aswan (under construction).

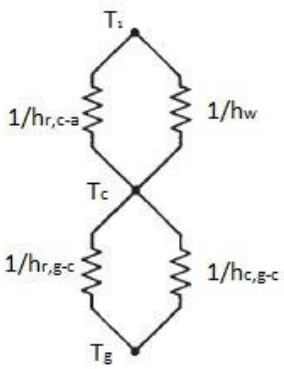

FIGURE 3. Thermal network for a collector in terms of convection, and radiation resistances.

from the mathematical model were compared with the Manzanares experimental results for a model validation and the model was further used to predict the performance characteristics of solar chimneys with its dimensions. Based on the proposed numerical approach, the effects of solar radiation, the pressure extracted at the turbine, and mass flow rate on the SCPP system performance were investigated in detail.

2. Mathematical model

According to the operation principle mentioned above, the air inside the collector is heated by solar radiation (greenhouse effect). The analysis used in this paper is based on the following simplifying assumptions:

- the uniform heating of the collector surface in terms of the sun's altitude angle is neglected;
- the frictional effect is ignored, since the velocity in this region is quite low;
- the flow in the collector is considered as a flow between two parallel plates;
- the heat losses through the wall of the chimney are neglected;
- the flowing humid air is considered as an ideal gas.

3. Mathematical model of solar collector

A solar collector is a special kind of a heat exchanger that transforms solar radiant energy into heat. The flux of incident radiation is a variable that can reach up to approximately $1100\,\mathrm{W/m^2}$ without optical concentration. The wavelength range is from 0.3 to 3.0 µm, which is considerably shorter than that of the emitted radiation from most energy-absorbing surfaces [14]. Thus, the analysis of solar collectors presents unique problems of low and variable energy fluxes and the relatively large importance of the radiation. In a steady state, the performance of a solar collector is described by an energy balance that indicates the distribution of incident solar energy into useful energy gain, thermal losses, and optical losses. The solar radiation absorbed by a collector per unit area of absorber I is equal to the difference between the incident solar radiation and the optical losses:

$$q_{\mathrm{add}} = I(\alpha_{\mathrm{g}}) - U_{\mathrm{t}}\Delta T = \frac{\dot{m}}{A_{\mathrm{c}}} C_{\mathrm{P}} \Delta T, \tag{1}$$

where α_{g} is the absorptivity of the glass cover, U_{t} is Collector loss coefficient ($\mathrm{W/m^2\,K}$), ΔT is the temperature difference between the air inside and outside of a solar collector, $\dot{m}$ is mass flow rate through the SCPP, and A_{c} is the area of the collector.

The energy loss through the top of the transparent cover is considered as the result of convection and radiation between parallel plates. The steady-state energy transfer between the plate at T_1 (ambient condition) and the cover at T_{c} is the same as between the cover and ground surface. The overall loss coefficient for a solar collector is for simplifying the mathematics of nonlinear equations. Consider the thermal network of a collector system shown in Figure 3. The resistance from the top cover to the surroundings has the convection heat transfer coefficient hw, which can be written as [14]

$$h_{\mathrm{w}} = 5.7 + 3.8 V_{\infty}, \tag{2}$$

where V_{∞} is the velocity of the surrounding air.

The radiation coefficient for the cover to the air $h_{\mathrm{r,c-a}}$ is given as

$$h_{\mathrm{r,c-a}} = \sigma \varepsilon_{\mathrm{g}} (T_{\mathrm{c}}^2 + T_{\mathrm{s}}^2)(T_{\mathrm{c}} + T_{\mathrm{s}}), \tag{3}$$

where σ is Stefan-Boltzmann constant ($5.6697 \cdot 10^{-8}\,\mathrm{W/m^2\,K^4}$), ε_{g} is the emittance between the sky and the ground and refers to the heat received by the ground, and T_{s} is calculated from the approximate model in reference [9]. The convection coefficient between the ground and the cover $h_{\mathrm{c,g-c}}$ can be found using

$$h_{\mathrm{c,g-c}} = \frac{Nu\,k}{L}, \tag{4}$$

where Nu is Nusselt number.

The radiation heat transfer coefficients between two parallel plates is given as

$$h_{\mathrm{r,g-c}} = \sigma \frac{(T_{\mathrm{g}}^2 - T_{\mathrm{c}}^2)(T_{\mathrm{g}} - T_{\mathrm{c}})}{\varepsilon_{\mathrm{g}}^{-1} + \varepsilon_{\mathrm{c}}^{-1} - 1}. \tag{5}$$

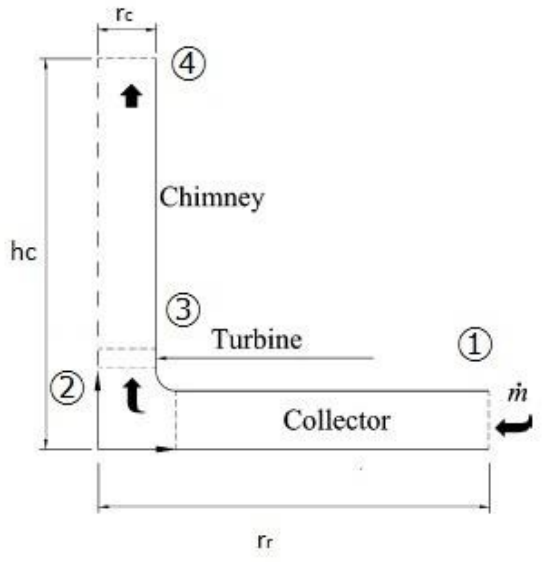

FIGURE 4. Schematic layout of the SCPP.

The top loss coefficient from the collector plate to the ambient is given from the thermal network

$$U_{\mathrm{t}} = \Big(\frac{1}{h_{\mathrm{w}} + h_{\mathrm{r,c-a}}} + \frac{1}{h_{\mathrm{c,g-c}} + h_{\mathrm{r,g-c}}}\Big)^{-1}. \qquad (6)$$

The procedure for solving the top loss coefficient using (1)–(6) is necessarily an iterative process. First, a guess is made from the unknown cover temperatures, from which the convective and radiative heat transfer coefficients between parallel surfaces are calculated. With these estimates, (6) can be solved for the top loss coefficient. The top heat loss is the top loss coefficient times the overall temperature difference, and since the energy exchange between plates must be equal to the overall heat loss. Figure 4 shows the points that should be calculated to obtain the performance of the SCPP. Point 1 is an ambient condition of the surrounding air.

To calculate the condition at the point 2, the equations for continuity, momentum and energy of the flow under the roof were applied by [13], which is written as:

$$p_2 = p_1 + \frac{\dot{m} q_{\mathrm{add}}}{2\pi h_{\mathrm{r}}^2 \varrho_1 C_{\mathrm{p}} T_1} \ln\frac{r_{\mathrm{r}}}{r_{\mathrm{c}}} - \frac{\dot{m}^2}{2\varrho_1}\Big(\frac{1}{A_2^2} - \frac{1}{A_1^2}\Big). \qquad (7)$$

By rearranging (1), the temperature at Point 2 can be obtained:

$$T_2 = T_1 + \frac{\alpha_{\mathrm{g}} I}{\frac{\dot{m} C_{\mathrm{p}}}{A_{\mathrm{r}}} + U_{\mathrm{t}}}. \qquad (8)$$

4. Mathematical model of solar chimney

The chimney or tower tube converts the heat absorbed by the solar collector into kinetic energy. The chimney utilizes the temperature difference between the cold air at the top and the heated air at the bottom. The pressure and temperature variation of the air inside the chimney is calculated considering an adiabatic expansion process, and written as:

$$T_4 = T_3 - \frac{g}{C_{\mathrm{p}}}, \qquad (9)$$

$$p_4 = p_1\Big(1 - \frac{g}{C_{\mathrm{p}} T_1} h_{\mathrm{c}}\Big)^{\frac{C_{\mathrm{p}}}{R}}. \qquad (10)$$

Point 4 is already obtained by using the outlet condition of the chimney (pressure p_4 and temperature T_4), then, a backward calculation is returned to obtain Point 3. Therefore, by rearranging the momentum and continuity equations for the flow through a constant area vertical tower of height hc, the maximum pressure difference throughout the solar chimney can be written as [15]:

$$\Delta p_{\max} = \frac{\varrho_1 g h_{\mathrm{c}} \Delta T}{T_1 + \Delta T} \qquad (11)$$

and

$$p_3 = p_4 + \frac{1}{2}(\varrho_3 + \varrho_4) g h_{\mathrm{c}} + \Big(\frac{\dot{m}^2}{A_{\mathrm{c}}}\Big)\Big(\frac{1}{\varrho_4} - \frac{1}{\varrho_3}\Big). \qquad (12)$$

By applying Bernoulli's equation for simplicity in Eqn. 12, the important formula for the maximum air velocity at the chimney's entrance is simplified to:

$$u_{\max} = \sqrt{\frac{2 g h_{\mathrm{c}} \Delta T}{T_1 + \Delta T}}. \qquad (13)$$

If the work extraction process at the turbine is assumed to be an isentropic process, then

$$T_3 = T_2\Big(\frac{p_3}{p_4}\Big)^{\frac{k-1}{k}}. \qquad (14)$$

5. Mathematical model of turbine

The turbine of the solar chimney is an important part of the SCPP system, which extracts the energy from the hot air and transmits it to the generator. The typical solar chimney turbine is of the axial flow type. It has characteristics between those of wind turbines and gas turbines [16]. It has significant influence on the system as the turbine pressure drop and plant mass flow rate are coupled. Thus, the pressure drop across the turbine can be expressed as a function of the total pressure difference, by neglecting friction losses, it can be written as:

$$\Delta p_{\mathrm{tur}} = \Delta p_{\mathrm{tot}} - \Delta p_{\mathrm{dyn}}. \qquad (15)$$

where Δp_{tot} is the available driving pressure that is calculated by $\frac{1}{2}\varrho u_{\max}^2$ and Δp_{dyn} is the dynamic pressure that is calculated by $\frac{1}{2}\varrho u_{\mathrm{with\ tur}}^2$. Let us denote the ratio $\Delta p_{\mathrm{tur}}/\Delta p_{\mathrm{tot}}$ as x, so that we get $u_{with\ tur} = u_{\max}\sqrt{1-x}$.

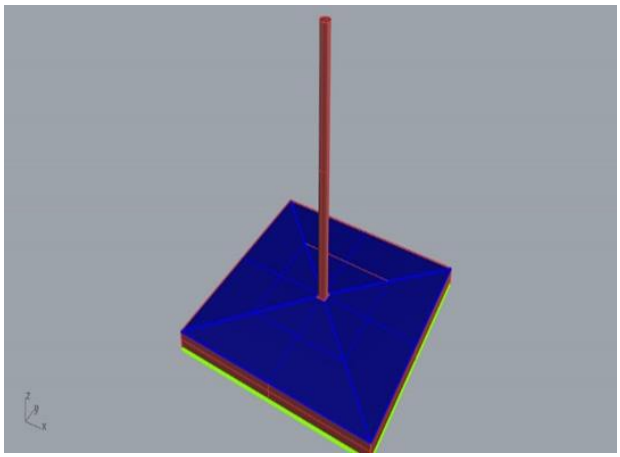

FIGURE 5. 3D SCPP geometry using Rhinoceros.

Rotational speed	300 rpm
Mass flow rate (same)	4 kg/s
Inlet total pressure	101336 Pa
Inlet total temperature	330.5 K
Total head rise	85 Pa

TABLE 1. Design conditions for Vista AFD.

The theoretical power extracted by the turbine can be determined from the energy equation and Gibbs relation from classical thermodynamics:

$$P = \dot{m} \int u \, \mathrm{d}p = \frac{\dot{m}}{\varrho_{\mathrm{tur}}} \Delta p_{\mathrm{tur}} = \frac{\dot{m}(p_2 - p_3)}{(\varrho_2 - \varrho_3)/2}. \quad (16)$$

Using x, the theoretical power can be written as:

$$P = A_{\mathrm{c}} u_{\max} \Delta p_{\mathrm{tot}} x \sqrt{1 - x}. \quad (17)$$

The optimal x for the maximum power extraction can be obtained by assuming that $u_{\max}$ and Δp_{tot} are not functions of x and solving $\frac{\partial P}{\partial x} = 0$. The result for the optimal pressure ratio is $2/3$.

According to the mathematical model described above, when the mass flow rate is assumed, then the power output can be obtained.

6. Computational work of a SCPP

The SCPP has many physical principles. The heating collector works as an air heater powered by solar energy, where all terms of heat transfer are applied to predict its performance. The heat transfer in the chimney tower is neglected, but buoyancy force is taken into account. The CFD involves the numerical solution of the differential governing equations of fluid flows and heat transfer. The ANSYS CFX v15 is used in the present study. The Reynolds's Averaged Navier-Stokes (RANS) equations for the compressible fluid flow are included in the equations of the conservation of mass and momentum. To solve the RANS, k–ω a turbulent model is chosen. Two radiation models are used, radiation heat transfer between the surfaces

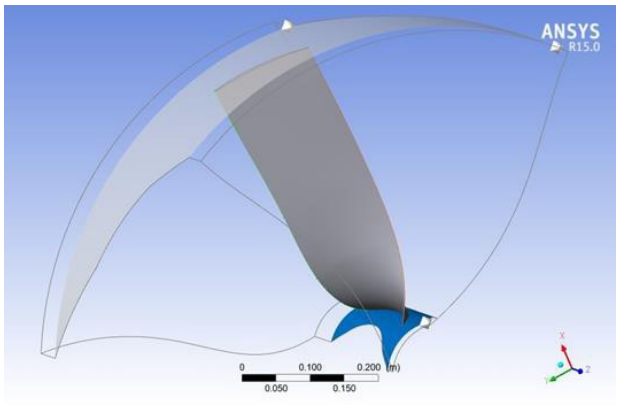

FIGURE 6. Turbogrid flow passage.

is carried out by the Monte Carlo model, and P1 radiation model is used in the fluid zone.

The SCPP unit consists of ground, cover collector, chimney and fluid zone. All component geometry is drawn in 3D using Rhinoceros 5.0, as shown in Figure 5. Grid generation is carried out using turbo grid. Vista AFD in ANSYS Workbench v15 is used to design the turbine. The MTFM (Matrix Through Flow Method) is applied to design the axial fan. However, the design of the turbine is carried out by entering the inlet flow condition as the output of the fan, and the outlet flow condition is an inlet of the fan. This condition is correct under the free vortex design for 0.5 degree of reaction. This condition allows reversing the turbomachine with consistent efficiency. The input aerodynamic parameter to Vista AFD is calculated from the free model of the SCPP. The parameters of the SCPP used to design the turbine are shown in Table 1.

For the turbine grid generation, the Turbogrid program is used. One passage of flow is generated and the flow regions hub, shroud, inlet and outlet are defined. Figure 6 shows the turbo grid passage that uses the H/J/C/L-grid to make the flow region and the O-grid closer to the blade surface.

7. Results of numerical analysis

To validate the mathematical model, the calculated results are compared with the experimental results of the prototype of the Manzanares. The measured data on September 2nd, 1982 are adopted from the reference [17]. The comparisons between the mathematical predictions results and the experimental values are presented in Table 2. There is a good agreement between the measurement and calculation results. The deviation of the collector loss coefficient, collector exit temperature, and output power are 4.95 %, 5.943 % and 0.816 % respectively, which are acceptable values.

Based on the plant dimensions and the mathematical model, Figure 7 shows the calculated power output as a function of the mass flow rate and solar radiation. As it can be seen from the figure, the increase of solar radiation increases the ability of mass rate, thus

	Measured	Calculated
Collector loss coefficient U_t (W/m^2 K)	15	15.7426
Temperature at collector exit T_2 (°C)	38	40.2583
Power P (kW)	48.4	48.795

Table 2. Comparison between measured data and mathematical model results.

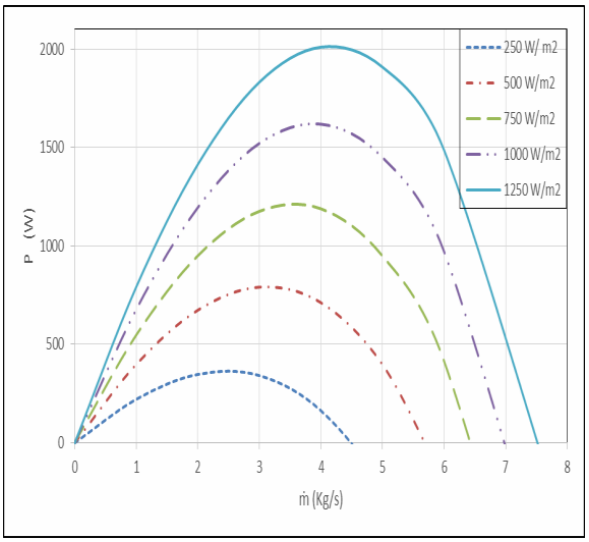

Figure 7. Influence of mass flow rate, and solar radiation on power output.

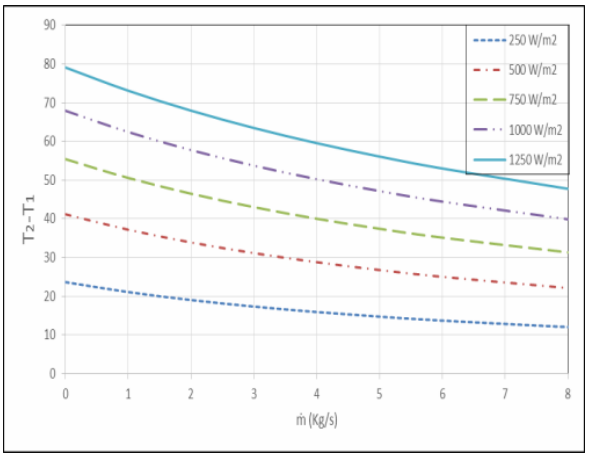

Figure 8. Influence of mass flow rate, and solar radiation on increasing temperature in collector.

	CFD	1D
Output power P (kW)	1670	1680
Upwind velocity u (m/s)	4.55236	4.566

Table 3. Comparison between CFD results and mathematical model results.

increase the output power. However, the maximum mass flow is 2.5 kg/s to 4 kg/s, which achieves the maximum output power of 2 kW at solar radiation of 1250 W/m^2.

The collector efficiency is measured by the temperature rise through it, and the temperature difference is a significant parameter of the SCPP performance. Figure 8 shows the influence of mass flow rate and solar radiation on increasing temperature in the collector. The solar radiation has a significant effect on the temperature difference in the collector. This difference reaches about 32 °C at a solar radiation of 1250 W/m^2. Details of the flow through the SCPP are obtained using the ANSYS CFX v15. Moreover, comparison between the CFX results and the mathematical model is done to ensure the accuracy of the CFD model. The calculation of the CFD and 1D models are used for solar radiation that has an average value on Saturday, June 6, 2015 ($I = 1050$ W/m^2) and Mass flow rate ($\dot{m} = 4$ kg/s) keeping other parameters constant. Table 3 shows the comparison between the CFD results and mathematical model results.

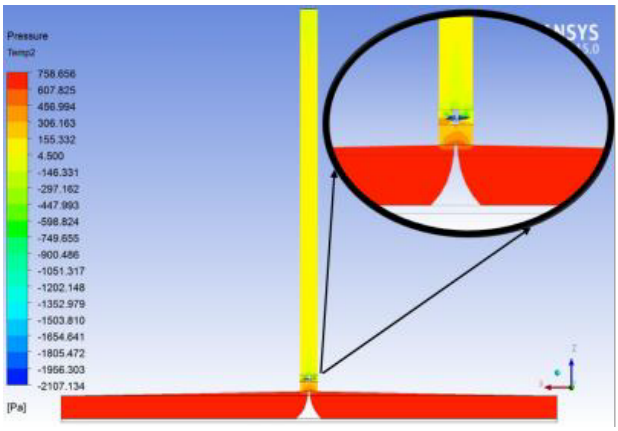

Figure 9. Contours of static pressure.

Figure 9 illustrates the contours of the pressure distribution at different zones of the chimney in a vertical cross section. The pressure around the turbine has a significant influence on the SCPP performance. Figure 10 shows that the pressure decreases through the turbine due to energy conversion. The heating air inside the collector is revealed by contours of static temperature as shown in Figure 11. Near the collector cover, it indicates that the ground temperature increases along the radial direction of the collector. This figure also demonstrates that ground temperature is higher than air flow temperature. Near the collector outlet, the temperature at the surface of the ground shows a slight drop in mid flow and then a sudden increase. According to [18], this is attributed to the high heat transfer coefficients present near the collector centre resulting from the higher collector air velocities in this area.

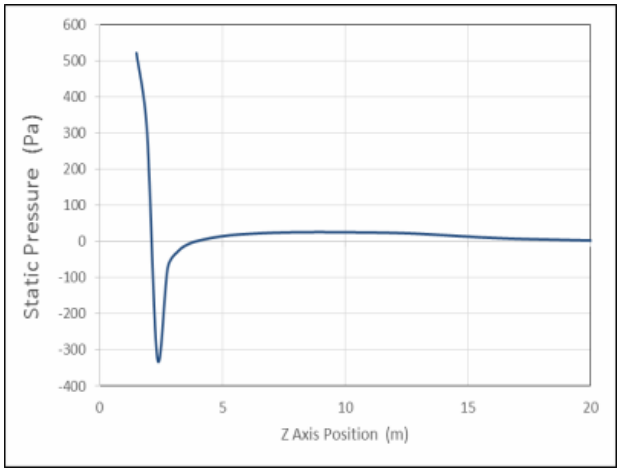

FIGURE 10. Pressure distribution inside the chimney.

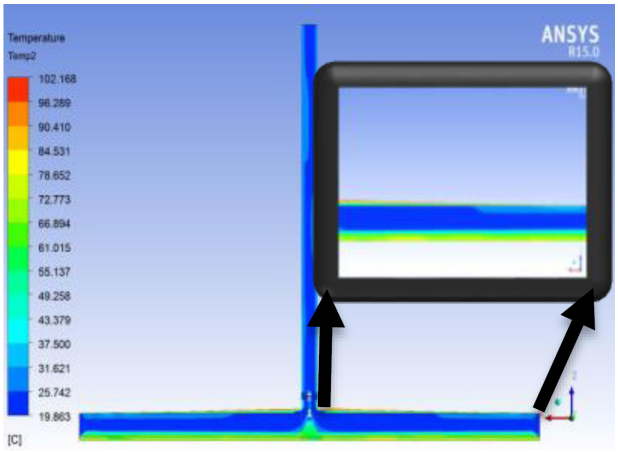

FIGURE 11. Contours of static temperature.

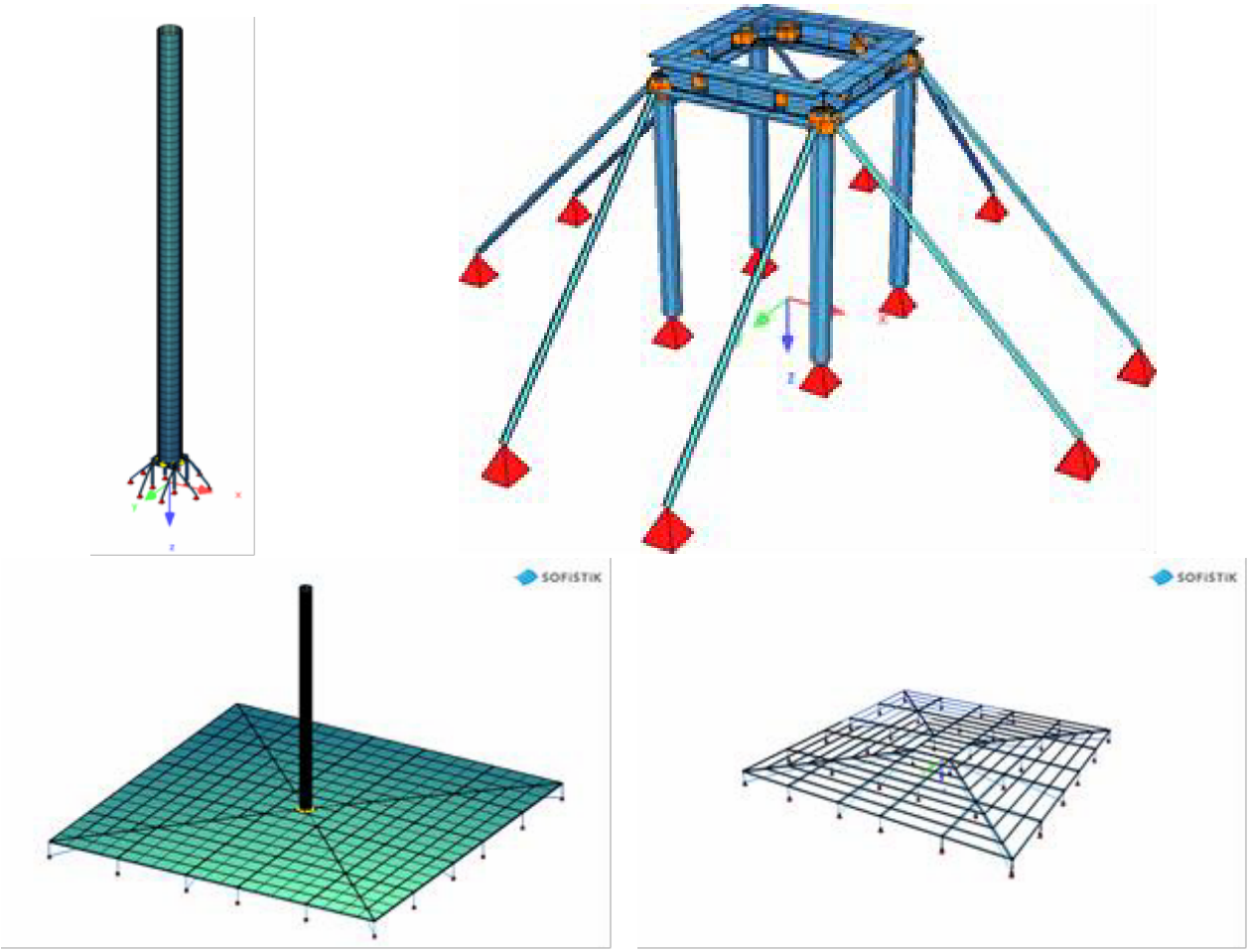

FIGURE 12. Numerical Model of SCPP: (top left) tower with supporting structure; (top right) supporting structure; (bottom left) solar tower and collector roof; (bottom right) collector roof without glass panels.

8. Design of solar chimney at Aswan, Egypt

Figure 12 depicts the FE-Model of the SCPP at Aswan, Egypt. The tower and supporting structure is made from S 235 steel with welded joints. The collector roof is made from standard glass panels with quadratic shape ($L = 1480\,\mathrm{mm}$). Due to reasons of simplicity, the collector roof is shaped as a four sided pyramid, which allows the use of plain glass panels instead of bent ones. Publications with a similar concept can be found at [19, 20].

9. Static calculations of solar tower and collector roof

Some results of the dynamic analysis of the designed solar tower will be discussed here. With a height to diameter ratio (H/d) of 20, the tower behaves more like a chimney than a shell structure. This can also be seen at the eigenfrequency and eigenmode, which are shown in Figure 13. The non-scaled SCPP with heights up to 750 to 1000 m will have a H/d ratio close to 10, which results in a more shell-like structure, cf. cooling towers. A few publications in this field of research will be mentioned here [21–24]. The whole analysis of the tower and collector can be found at the report for 2015 [25].

10. Structural health monitoring (SHM) concept

The growing interest in the practical implementation of various Structural Health Monitoring (SHM) strategies on full scale structures lies in the potential of these methodologies to detect significant deteriorations of a structure in their initial stages [26]. As a result, this allows a timely action to be taken, minimizing the maintenance costs and shut-down time of the system.

As one of the most common SHM strategies, vibration based structural health monitoring is capable of delivering valuable information on structural changes. But in order to build a reasonable and effective monitoring system that is capable of capturing all the necessary phenomena, it is important to consider, during the monitoring system design, the decisions concerning the type, number and strategic positioning of sensors, adequate sampling frequencies and quantity of recorded signals as well as proper data storage tools and equipment.

11. SHM framework for continuous monitoring

In the current case study for a solar chimney plant, a three-step SHM strategy for the detection of structural changes was developed. Within this paper, the preliminary Operational Modal Analysis (OMA) estimates for the test case as well as the first steps towards a long-term monitoring campaign of a solar chimney plant are presented.

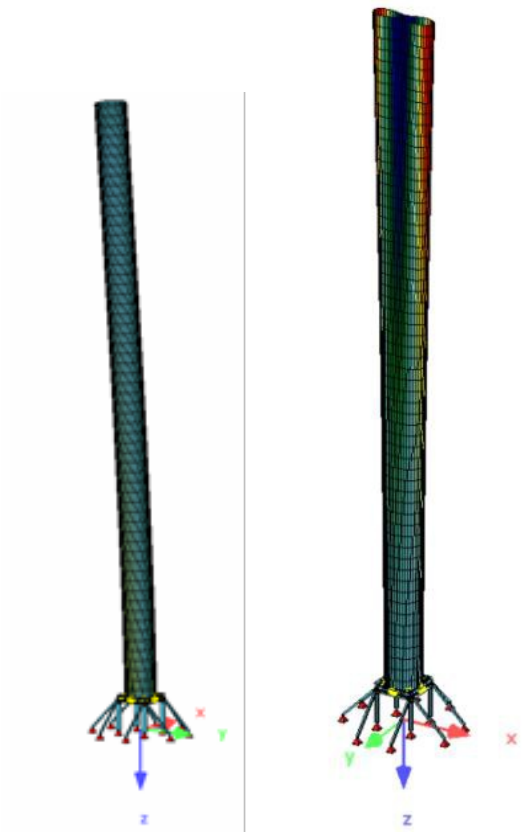

Figure 13. Eigenmode with Eigenfrequency: (left) beam mode, $f_1 = 1.80\,\mathrm{Hz}$; (right) shell mode, $f_3 = 21.84\,\mathrm{Hz}$.

The proposed continuous SHM concept is based on the well-proven system response (output only) monitoring that can provide the necessary information for early recognition of changes in the structural behaviour due to damage or significant deterioration. This approach, also known as the OMA, has been successfully implemented for a system identification of large scale civil structures, where the classical experimental modal analysis is not possible to implement, as it is not possible to measure the input forces [27]. But with the OMA, it is possible to perform a system identification only from the measured responses. An overall SHM procedure consists of: a development and implementation of a monitoring system, safe storage and handling of the data and finally data processing and post processing.

The three step proposed SHM concept detects the structural changes in three stages, as summarized in Figure 14. The first stage is from a direct observation of the real time history statistical data, in most cases 10 minute mean, maximum, minimum and standard deviation. In this step, it is very important to initially determine the threshold limits of all sensors for different environmental and operational conditions during the first year continuous monitoring of the structure. This method works well as the structure is, in most cases, considered to stay undamaged during its first year of service.

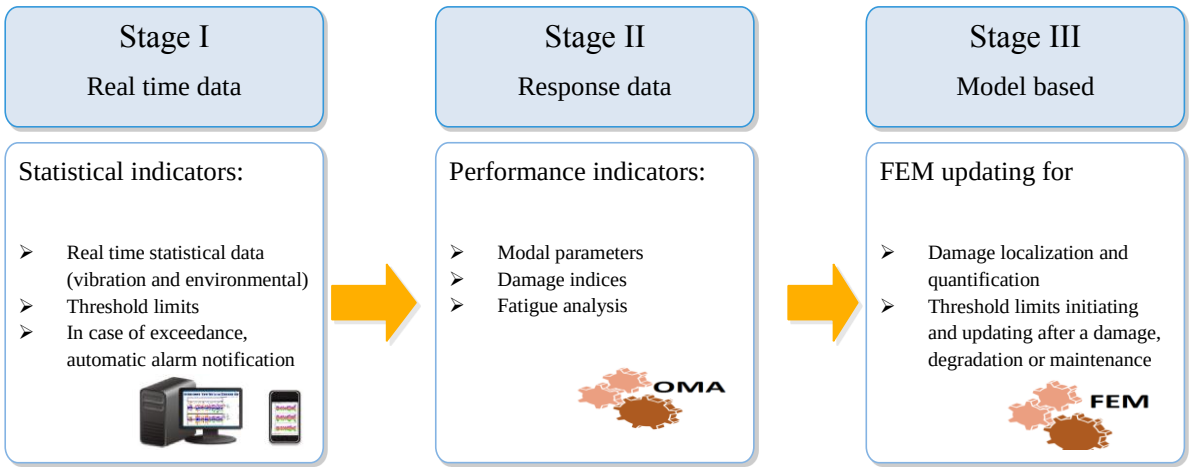

FIGURE 14. SHM strategy for continuous monitoring of operating slender structures (Airwerk GmbH).

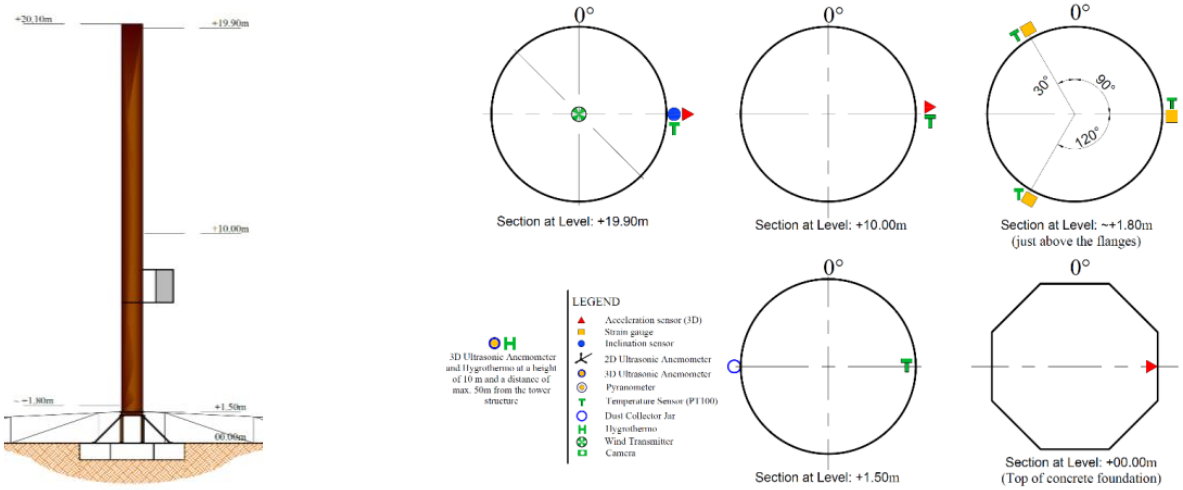

FIGURE 15. Sensor positions and layout.

The second stage is by processing of the monitoring data to determine the global structural modal parameters (natural frequencies, mode shapes and modal damping) and the fatigue analysis from the stress time history data. Also, in this step, the reference modal parameters of the healthy structure need to be determined during the early monitoring stage, so that they will serve as references for the remaining lifetime of the structure. Based on measured stress time histories, a fatigue analysis (by rain flow counting) is performed, for estimating the remaining service lifetime of the structure as well as for possible extension of the structure's service life time beyond its design life with minimum risk.

The third stage is a model based damage location and quantification. In this step, an FE model of the built structure will be prepared and calibrated from the initially obtained healthy state parameters. In this calibrated FE model, possible expected damage scenarios can be simulated so as to observe the variation in the parameters being computed in the first and second stages. Then, the threshold limits can be established to be later used for the damage location and quantification by adding up the information obtained in all three steps. This FE model will be continuously updated with the varying parameters due to structural damage, degradation or maintenances.

12. PROPOSED SENSOR POSITIONS

Using the previously described three-stage concept (Figure 14), an array of sensors was initially proposed, which was later revised due to financial constraints to fully implement it. Considering that this is a research project, the initially proposed concept was made so as to allow for system redundancy. Due to the very high temperatures the sensors will be exposed to, a cross checking the response of more than one sensor when a significant structural change occurs will be made to enhance the reliability of the data.

As shown in the latest revised sensor positions in Figure 15, the used sensors can generally be classified

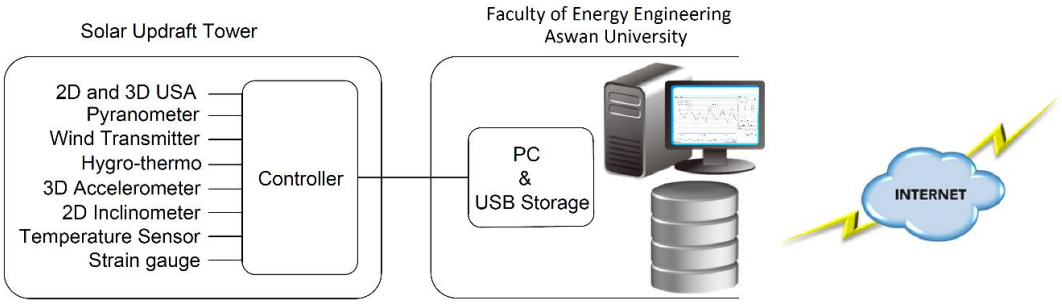

Figure 16. General overview of network diagram.

as structural and environmental sensors. Three 3D accelerometers are used; one at the top, one at the middle of the tower, and the third one on the top of the concrete foundation to measure the ground motion from seismic activity. One 2D inclinometer is used at the top of the tower to measure inclinations. At the bottom of the tower structure, just above the stiffeners, three rosette type strain gauges are to be installed at an angle of 120° to each other, so that it is possible to compute the principal stresses, orientation of principal stresses, shear stress, and also to record the strain time history for fatigue analysis.

13. Implementation and expected results

After all the sensors are installed in position, all their channels are to be connected with the I/O modules inside the steel cabinet mounted on the outside surface of the tower (Figure 15). All sensors are to be provided with adequate supports to protect them against physical and environmental damages. Cable routing is also to be done in consideration of the protection of the cables from damages that may result from exposure to extreme heat and physical forces.

All the I/O modules are in turn connected to the controller (data logger) housed in the cabinet. Then, finally, all the data are to be transferred to the computer inside the faculty of Energy Engineering, Aswan University (Figure 16).

This computer will serve as a server, where the monitoring data are stored. A web interface is also to be developed, which enables real time data visualization, along with the possibility to select particular channels to visualize. Also, with the possibility to download a selected data range. LAN ports will be required on the server location (the university) for remote access, manipulating and maintaining the data acquisition system.

The results expected from this monitoring system are the real time data visualization, including correlation of the responses from sensors among themselves and with environmental conditions. Also, once the threshold limits are defined, an automatic alarm notification can be implemented, which sends automatic notification via email or SMS. The data obtained from the accelerometers will be used to extract the modal parameters by using operational modal analysis technique, which makes use of only the output data. The strain time history data recorded by the strain gauges will be used to compute the principal stresses, bending moments and for performing fatigue analysis using the rain flow counting method [28].

This Solar Chimney Project in Aswan, although it is a small scale research project, can serve as an ideal experimental field for future commercial implementation of the already designed large solar updraft towers, some of them reaching up to a height of about 1000m and higher [29].

	Parameter	**Value** (m)
Tower	Height	1
	Diameter	0.15
	Thickness	0.003
Collector	Perspex Sheet B × L	1.40 × 1.90
	Thickness	0.005

Table 4. Parameter of Wind Tunnel Setup.

14. Wind tunnel model

Wind tunnel tests shall give some information about the flow structure inside the transition section. The flow will be redirected from a nearly horizontal flow underneath the solar collector into a vertical flow inside the solar chimney. Therefore, an experimental model has been built at the wind tunnel in Stellenbosch, South Africa. Details about the used wind tunnel can be seen in [30]. The model shows, in a simplified manner, a solar chimney with a rectangular collector roof, Figure 17. The influence of turbines has not been taken into account, instead, eight openings inside the tower wall represent the flow inlets through the turbines. Local influence onto the flow situation due to the turbines will be neglected. Main model dimensions are shown in Table 4.

The wind tunnel test section is equipped with two walls made of Perspex, which enables the use of a PIV system positioned on the outside of the wind tunnel. The top end of the cylinder was connected to a venturi flow meter and a fan to get defined mass flow rates

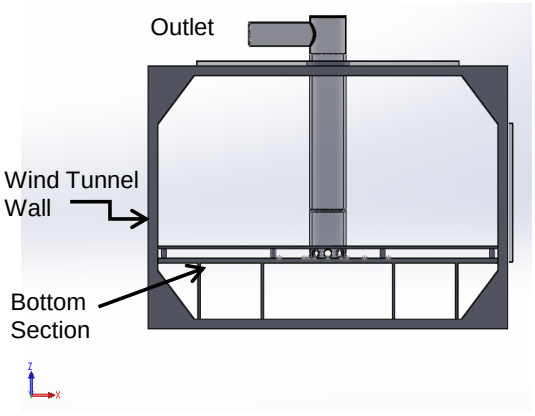

a) Windward Side

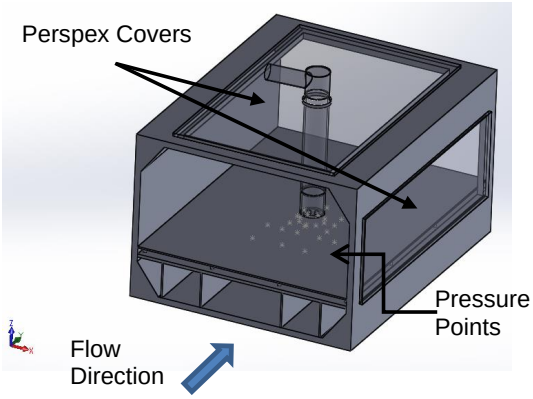

b) Isometric View from Windward Side

c) Fan and Venturi Flow Meter

d) PIV Equipment

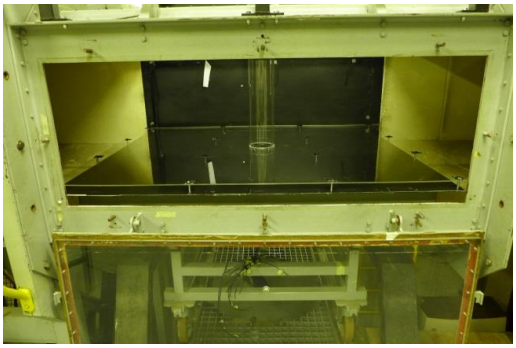

e) Test Section and Model I

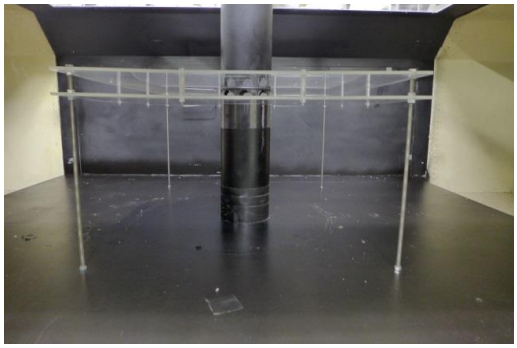

f) Modell II

FIGURE 17. Experimental Setup.

through the tower, Figure 17c. Local temperature and static pressure has been taken from measuring points inside the wind tunnel facility, respectively. Additional pressure measurements shall give some information about the pressure situation underneath the solar collector and inside the solar tower close to the flow inlets. All in all, up to 40 pressure points, inserted flush to the bottom section, give some good distribution and spatial resolution. Figure 17d shows the installation of the PIV system for measuring a horizontal layer just in the middle, between the solar collector and the bottom section. The cameras can be seen on top of the wind tunnel facing downwards. Using two cameras enabled us to measure overlapping flow areas, which has been advantageous for the evaluation of the measured data. Figure 17ef depict the wind tunnel model I and II. The difference is in the position of the Perspex sheet representing the solar roof. In variant I, the 5 mm Perspex sheet has been installed in a distance of 40 mm from the bottom sec-

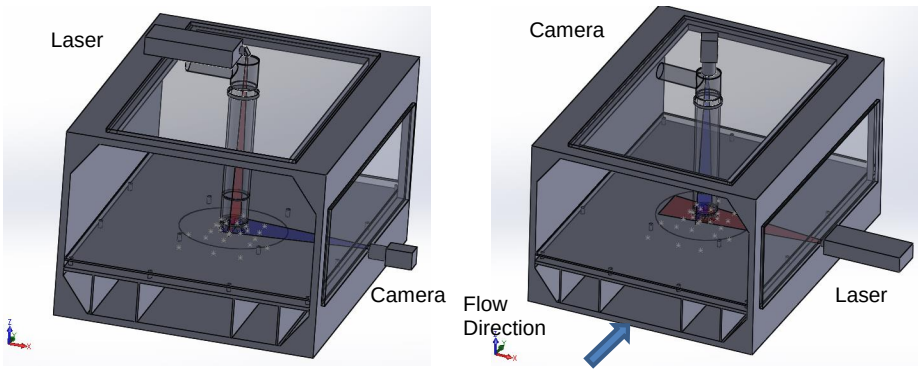

Figure 18. Configuration of PIV Measurements (Variant I): (left) Configuration I — vertical laser plain; (right) Configuration II (horizontal laser plain).

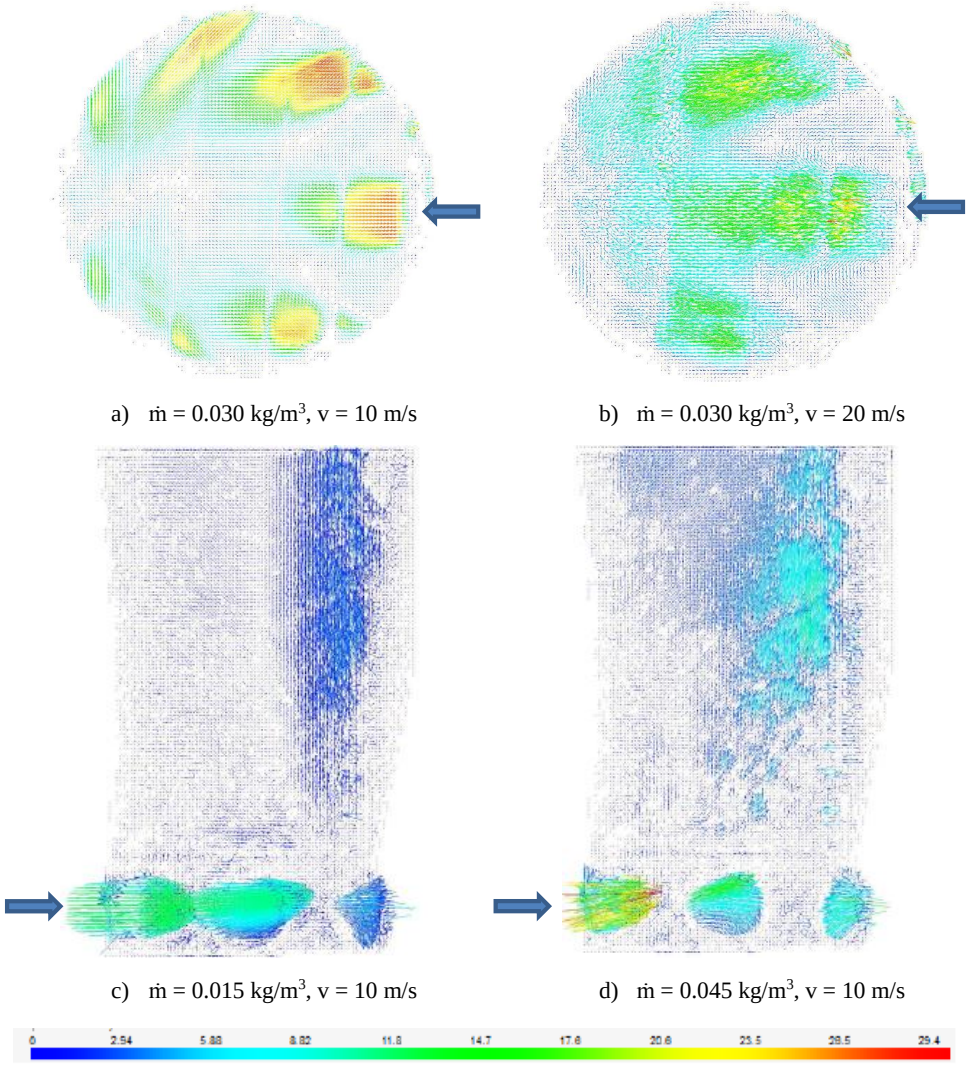

Figure 19. Mean Velocity Vectors in m/s for horizontal and vertical plain.

tion with sizes mentioned in Table 4. Based on the first results gained from the variant I, the Perspex sheet has been moved to a middle position inside the wind tunnel ($z = 380\,\text{mm}$, above bottom section) and now consists of a top and bottom sheet. The dimensions (length and width direction) have been changed respectively.

15. Installation of particle image velocimetry (PIV) equipment

For a better understanding of the flow situation underneath the solar collector and on the inside of the solar tower, the PIV measurements have been performed, including two horizontal and two vertical

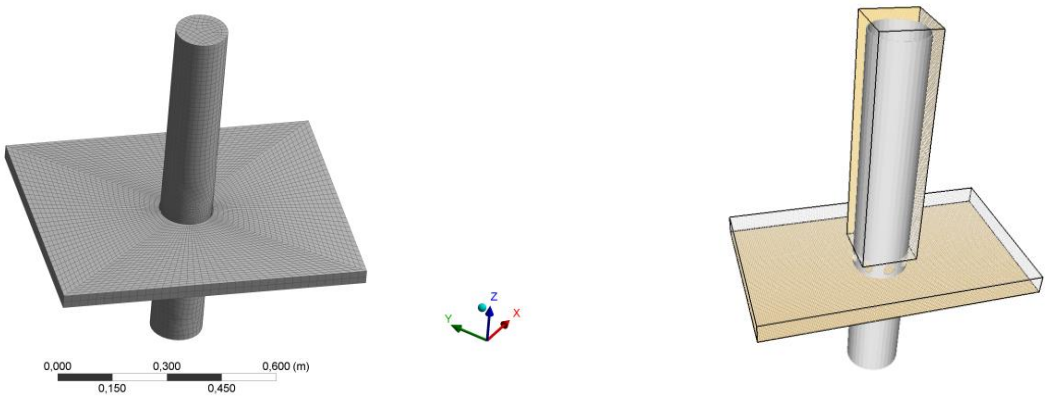

FIGURE 20. CFD Model of Experimental Setup from Stellenbosch: (left) ANSYS Fluent (generic); (right) Fire Dynamics Simulator (FDS).

plains. A DualPower Laser and two FlowSense 4M cameras from DantecDynamics® have been used. The evaluation of the measured data has been carried out with DynamicStudio v3.41. Figure 18 depicts the general setup for the variant I.

16. Results of PIV measurements

Some results from the performed PIV measurements are shown in Figure 19. For a spatial resolution, two horizontal and two vertical plains have been investigated. Only the mid-plain between the solar collector and the bottom section and the solar tower are depicted here. Three free stream velocities v and three mass flow rates $\dot{m}$ inside the solar tower give some insight into the flow situation. Results show velocity vectors of filtered mean values. For the horizontal plain, the flow direction is from right to left and turned around for the vertical plain.

All four results show the influence of v and $\dot{m}$ on the flow distribution, mainly inside the transition section. The vectors in the horizontal plain with varying free stream velocities show a clear image of the streams through the openings at a smaller free stream velocity, Figure 19ab. This means that the influence of the flow through the tower is smaller with a higher free stream velocity. In Figure 19a, you can see seven and, in Figure 19b, only three major streams, which confirms the aforementioned conclusion. The same observation can be made from the vertical velocity vector plots in Figure 19cd. This time, the mass flow inside the tower has been changed instead. It can be seen that the stream is shifted towards the lee side with smaller mass flow $\dot{m}$ through the solar tower. Both results show the significant asymmetry of the flow inside the transition section, which could also be evoked through maintenance of one of the turbines. The aspect of symmetry has been taken as a simplification for all known publications to the current state. For this reason, the spatial resolution of the flow situation should be investigated in 3D model tests of the SCPP, to correctly understand the flow situation inside a solar chimney and get reliable results for the efficiency.

17. CFD analysis for validation and verification of wind tunnel tests

For numerical tests, a CFD model has been built with the commercial software ANSYS Fluent and the Fire Dynamics Simulator (FDS) software from NIST. The aim has been to find alternatives to the commercial software and to avoid huge computational performance due to grid sensitivity studies. The wind tunnel model, with its dimensions, has been taken as the reference. The validation and verification of a one-to-one model of the power plant at Aswan will be done in a second step.

18. CFD models

The CFD models with experimental dimensions are shown in Figure 20.

While the discretized mesh in the ANSYS Fluent consists of tetrahedral and hexahedral elements, the model in the FDS can only be modelled with quadrilateral elements. This allows a fast grid construction, because the user has to insert only the exact amount of elements in each direction. The depicted model consists of elements with side lengths of 5 mm in all three directions. A finer grid resolution has been built, but could not been solved due to the lack of computer performance. This advantage for many fluid mechanic problems has its shortcomings when it comes to round and circular structures. For this reason, it is only possible to generate round structures as a polygon, which should not be a problem when a local influence on the flow patterns can be neglected. For global solutions, this should not have a major influence on the results. This statement will be checked within further studies. First results show a good agreement with the conventional CFD codes.

19. Conclusions and further studies

(1.) The main objective is to evaluate the solar chimney performance theoretically. A mathematical model (1D) and the CFD model are used to estimate the temperature rise in the collector and pressure distribution of a solar chimney as well as to estimate the effect of various parameters on the power output. In addition, the mathematical model was validated with the experimental data from the prototype in Manzanares. The presented study shows that the capabilities of the CFD and mathematical model - powerful research tools for the analysis of a complex thermofluid flow in the SCPP [31].

(2.) In order to build a reasonable, but at the same time effective monitoring system that will capture all necessary phenomena, the optimization of types, number and strategic positioning of sensors, the required sampling frequency and quantity of recorded signals as well as proper data storage tools and equipment need to be considered. In this paper, planning strategies as well as preliminary data based estimates of the structural dynamics are discussed. The presented ongoing case study is targeted at vibration based structural health monitoring strategies capable of delivering valuable information on structural changes by utilizing features extracted only from the measured vibration structural response. The focus of a further research is a development of automated damage detection frameworks that will be able to alarm as soon as any structural damages occur. In turn, this allows taking timely action, minimizing the maintenance costs and down time of monitored systems.

(3.) The results of experimental and numerical simulations show that free stream velocity and spatial resolution have major effects on the flow situation inside the SCPP. Therefore, measurements on the SCPP at Aswan will be performed to investigate the effect on the flow field on the in- and outside and gain some new information about its global impact on the performance and efficiency. In a second step, new wind tunnel tests will be performed to verify, if there is an optimal installation inside the transition section to divert the flow from a horizontal to a vertical direction without much additional turbulence and loss of energy. The aim will be to increase the efficiency, so the principle can be applied to large scale power plants in near future.

Acknowledgements

All joint project partners want to express their gratitude to the Federal Ministry of Education and Research (BMBF), the Science and Technology Development Fund (STDF) of Egypt and the project leaders from DLR for their financial support.

References

[1] Comsan, M. *Solar energy perspectives in Egypt.* 4th Environmental Physics Conference, Hurghada, Egypt, 10-14 March (2010).

[2] Haaf, W., Friedrich, K., Mayr, G., Schlaich, J. *Solar chimneys Part I: Principle and construction of the pilot plant in Manzanares.* International Journal of Solar Energy, Vol. 2, p.3–20 (1983).

[3] Haaf, W. *Solar chimneys Part II: Preliminary test results from the Manzanares pilot plant.* International Journal of Solar Energy, Vol. 2, p.141 – 161 (1984).

[4] Lu, F., Zhang, H., Yao, X.P., et al. *Review of key technologies for solar chimney power generation.* East China Electric Power (2006).

[5] Huang, H., Zhang, H., Huang, Y., Lu, F. *Simulation calculation on solar chimney power plant system.* In International Conference on Power Engineering, Hangzhou, China (2007).

[6] Patel, S.K., Prasad, D., Ahmed, M.R. *Computational studies on the effect of geometric parameters on the performance of a solar chimney power plant.* Energy Conversion and Management, no. 77, p. 424–431 (2014).

[7] Vieira, R.S., Garcia, C., Junior, I.C.A., Souza, J.A., Rocha, L.A.O., Santos, L.A.I.a.E.D.d. *Numerical study of the influence of geometric parameters on the avaliable power in a solar chimney.* Thermal Engineering, vol. 14, no. 1, p.103-109 (2015).

[8] Pretorius, J., Kröger, D. *Solar chimney power plant performance.* Journal of Solar Energy Engineering, vol. 3, no. 128, p.302–311 (2006).

[9] Bernardes, M., Voss, A., Weinrebe, G. *Thermal and technical analyses of solar chimneys.* Solar Energy, no. 75, p.511–524 (2003).

[10] Gannon, A., von Backström, T. *Solar chimney cycle analysis with system loss and solar collector performance.* Journal of Solar Energy Engineering, no. 122, p.133–137 (2000).

[11] Pasumarthi, N., Sherif, S. *Experimental and theoretical performance of a demonstration solar chimney model – Part I: Mathematical model development.* International Journal of Energy Research, no. 22, p.277–288 (1998).

[12] Pasumarthi, N., Sherif, S. *Experimental and theoretical performance of a demonstration solar chimney model – Part II: Experimental and theoretical results and economic analysis.* International Journal of Energy Research, no. 22, p.443–461 (1998).

[13] Koonsrisuk, A., Chitsomboon, T. *Mathematical modeling of solar chimney power plants.* Energy, no. 51, p. 314-322 (2013).

[14] Duffie, J.A., Beckman, W.A. *Solar engineering of thermal processes.* Hoboken, New Jersey: John Wiley & Sons, Inc. (2013).

[15] Krätzig, W.B. *Physics, computer simulation and optimization of thermo-fluidmechanical processes of solar updraft power plants.* Solar Energy, vol. 98, no. A, p.2-11 (2013).

[16] Von Backström, T., Gannon, A. *Solar chimney turbine characteristics.* In ISES 2001 Solar World Congress, Matieland, South Africa (2001).

[17] Weinrebe, G., Schiel, W. Up-draught solar chimney and down-draught energy tower – a comparison. In *ISES 2001 Solar World Congress*, Stuttgart, Germany, 2001.

[18] Dhahri, A., Omri, A., Orfi, J. *Numerical study of a solar chimney power plant.* Research Journal of Applied Sciences, Engineering and Technology, vol. 8, no. 18, p.1953-1965 (2014).

[19] Coetzee, H., Oram, C. *Solar chimney exit loss control by use of a diffuser (2005).*

[20] Krätzig, W.B., Niemann, H.-J., Harte, R., Höffer, R. *Solar updraft power plants experimental prototype with 350m solar chimney and square collector of 1km2 of area.* Bochum, Germany (2015).

[21] Lupi, F. *Structural behaviour, optimization and design of a solar chimney prototype under wind loading and other actions.* Master Thesis. Bochum, Germany, University of Bochum (2009).

[22] Van Eck, S.R.G. *Solar updraft tower – Structural optimization under dynamic wind action.* Master Thesis, Delft, The Netherlands, Delft University of Technology (2014).

[23] Witting, D. *Numerische Umsetzung und Untersuchung verschiedenartig modellierter Varianten eines SCPP in SOFiSTiK.* Wuppertal, Germany, University of Wuppertal (2016).

[24] Harte, R., Graffmann, M., Krätzig, W.B. *Optimization of solar updraft chimneys by nonlinear response analysis.* Applied Mechanics and Materials, Vol. 283, p.25 – 34 (2013).

[25] Harte, R., Höffer, R., Tschersich, M. *Solar Chimney Power Generation – Case of Aswan, Egypt.* Report for 2015, Project-ID: IB-023/ASW-SO-CH (2015).

[26] Doebling, S.W., Farrar, C.R., Prime, M.B., Shevitz, D.W. *Damage identification and health monitoring of structural and mechanical systems from changes in their vibration characteristics: a literature review.* Los Alamos National Laboratory report LA-13070-MS (1996).

[27] Brincker, R., Ventura, C.E., Andersen, P. *Why output-only testing is a desirable tool for a wide range of practical applications.* Proceedings of the IMAC-XX (2002).

[28] Höffer, R., Tewolde, S., Bogoevska, S., Baitsch, M., Zimmermann, S., Barbanti, G. *Monitoring based identification for structural life cycle management of wind energy converters, Europe and the Mediterranean towards a sustainable built environment.* SBE16 Malta (2016).

[29] Harte, R., Höffer, R., Krätzig, W.B., Mark, P., Niemann, H.-J. *Solar updraft power plants, Engineering structures for sustainable energy generation.* Engineering Structures 56, p.1698– 1706 (2013).

[30] Burger A.A.S. *Numerical analysis of flow around infinite and finite cylinders at trans-critical Reynolds numbers with and without surface roughness.* Master Thesis. Stellenbosch, South Africa, University of Stellenbosch (2015).

[31] Mekhail, T., Elmagid, W.M.A., Fathy, M., Bassily, M., Harte, R. *Theoretical investigation of solar chimney power plant installed in Aswan City.* Aswan City, Egypt: Aswan University (2016).